Wen *et al. Chem Synth* 2024;4:9
DOI: 10.20517/cs.2023.45

Chemical Synthesis

Research Article

Open Access

Catalyst-free solid-state cross-linking of covalent organic frameworks in confined space

Dan Wen[1,2], Saikat Das[3], Yu Zhao[1,2,3,*], Jingru Fu[1,2,3], Zelong Qiao[4], Yijing Gao[1,2], Yuxia Wang[3], Ziqiang Zhao[3], Dapeng Cao[4], Daoling Peng[5], Weidong Zhu[1,2], Teng Ben[1,2,3,*]

[1]Zhejiang Engineering Laboratory for Green Syntheses and Applications of Fluorine-Containing Specialty Chemicals, Institute of Advanced Fluorine-Containing Materials, Zhejiang Normal University, Jinhua 321004, Zhejiang, China.
[2]Key Laboratory of the Ministry of Education for Advanced Catalysis Materials, Institute of Physical Chemistry, Zhejiang Normal University, Jinhua 321004, Zhejiang, China.
[3]Department of Chemistry, Jilin University, Changchun 130012, Jilin, China.
[4]State Key Laboratory of Organic-Inorganic Composites, Beijing University of Chemical Technology, Beijing 100029, China.
[5]Key Laboratory of Theoretical Chemistry of Environment, Ministry of Education, School of Environment, South China Normal University, Guangzhou 510006, Guangdong, China.

[*]**Correspondence to:** Dr. Yu Zhao, Prof. Teng Ben, Zhejiang Engineering Laboratory for Green Syntheses and Applications of Fluorine-Containing Specialty Chemicals, Institute of Advanced Fluorine-Containing Materials, Zhejiang Normal University, 688 Yingbin Road, Jinhua 321004, Zhejiang, China. E-mail: zhaoyu@zjnu.edu.cn; tengben@zjnu.edu.cn

How to cite this article: Wen D, Das S, Zhao Y, Fu J, Qiao Z, Gao Y, Wang Y, Zhao Z, Cao D, Peng D, Zhu W, Ben T. Catalyst-free solid-state cross-linking of covalent organic frameworks in confined space. *Chem Synth* 2024;4:9. https://dx.doi.org/10.20517/cs.2023.45

Received: 16 Sep 2023 **First Decision:** 14 Dec 2023 **Revised:** 1 Jan 2024 **Accepted:** 8 Jan 2024 **Published:** 12 Jan 2024

Academic Editors: Bao-Lian Su, Feng Shi **Copy Editor:** Dong-Li Li **Production Editor:** Dong-Li Li

Abstract

A "confined space" provides a unique environment to regulate the crystallization thermodynamics and kinetics by confining the reactants in the restricted space dimensions. Solid-state crystal-to-crystal transitions in confined space are controlled by the preassembly of molecules in a crystal lattice and occur inside the lattice. Herein, we report the first case of construction of crystalline cross-linked covalent organic frameworks (CL-COFs) through solid-state cross-linking of acetylenic groups-bridged 2D COFs in spatially limited systems. Specifically, this transformation is thermally induced, yielding CL-COFs with superlative properties, including outstanding enhancement in crystallinity, specific surface area, and stability. We further demonstrate the CL-COFs as high conductivity polymers after iodine doping. This work underscores the opportunity to use lattice-constrained solid-state cross-linking to develop more versatile and feature-rich polyacetylene networks.

Keywords: Solid-state cross-linking, covalent organic frameworks, cross-linked covalent organic frameworks, conducting materials

INTRODUCTION

Polyacetylene has attracted extensive attention due to its interesting properties such as electrical, optical, and magnetic properties and has become an important research topic in the field of conjugated organic polymers throughout its long history[1-5]. In fact, early investigations on acetylene polymerization did not result in a linear conjugated polymer but, instead, a three-dimensional cross-linked organic polymer referred to as cuprene[6,7]. However, differences in starting materials and preparation methods resulted in too complex and poorly defined structures and compositions of these materials[8]. Greater efforts have turned to the preparation of similar conjugated polymer systems with well-defined and controllable compositions. In 1958, Natta *et al.* achieved the first polymerization of acetylene by organometallic catalysis[9]. However, the polyacetylene powder they prepared was completely insoluble and infusible. It was not until 1977 that Shirakawa *et al.* succeeded in the direct polymerization of acetylene to form thin films; this groundbreaking discovery aroused great interest in synthetic metals[1]. Cyclic polyacetylene, as another form, has also been developed rapidly during the same period. Since Reppe and Schweckendiek reported the transition-metal catalyzed [2 + 2 + 2] cyclotrimerization of alkynes to form aromatic ring structures[10], researchers became eager to challenge the limits of aromatic ring size basic formula $(CH)_n$[11,12]. In 2021, Miao *et al.* first reported the catalytic synthesis of [∞]annulene with impressively low defects, highly conjugated structures, and low free-electron density [Scheme 1A][13]. However, the polymerizations involved in the previous efforts have often been accompanied by some of the following problems: (i) the reaction requires a large number of expensive and environmentally unfriendly metal catalysts; (ii) the polymerization conditions are harsh and the operation is cumbersome; and (iii) air sensitivity and poor stability have hampered the commercial success of polyacetylene.

Solid-state polymerization (SSP) has provided a promising solution because it can force chemical reactions to proceed with a minimum amount of atomic and molecular movement through solid-state confinement and preorganization[14-16]. Due to the lack of solvation, the reactants are almost "naked" in a confined space and ready for reaction with lower activation energy[17-19]. Therefore, SSP can occur without additional catalysis[20]. To the best of our knowledge, direct polymerized acetylenic groups to form a crystalline polymer without the addition of a catalyst is unprecedented and inconceivable. It would, thus, be of general interest to develop an efficient method for the polymerization of acetylenic groups in crystals.

As an emerging class of highly crystalline porous materials, covalent organic frameworks (COFs) are an ideal platform for solid-state reactions in the confined space[21-29]. Huang *et al.* reported, for the first time, the interlayer [4 + 4] cycloaddition reactions in borate-linked anthracene 2D COFs, realizing the smart light response of COFs[30]. Acharjya *et al.* showed that UV/Vis light irradiation [2 + 2] cycloaddition reaction of vinyl COF realized the transformation from 2D to 3D. However, during this process, the sp^2 hybridized vinyl carbon in the skeleton was converted to sp^3-cyclobutane species, and the product lost crystallization[31]. A recent study by Jadhav *et al.* showed that the degree of polymerization and crystallinity of the vinyl [2 + 2] cycloaddition in COFs is affected by the dispersed solvent, low to medium polar aprotic solvents are more likely to form crystalline products[32]. Besides photoinitiation, thermal initiation is also an effective method to induce SSP. In 2021, Zhu *et al.* reported thermally induced construction of interlayer conjugated links via SSP in diacetylene-contained COFs, which provided an efficient paradigm for conducting SSP[33].

Herein, we report, to the best of our knowledge, the first case of solid-state reaction in the confined space to construct cross-linked (CL)-COFs in acetylene bridged 2D COFs [Scheme 1B], and this cross-linking reaction does not require any catalyst. Our strategy is to use acetylenic groups (–C≡C–) to construct a series of 2D COFs and use face-to-face π-stacking interaction to make the adjacent acetylenic groups at a suitable

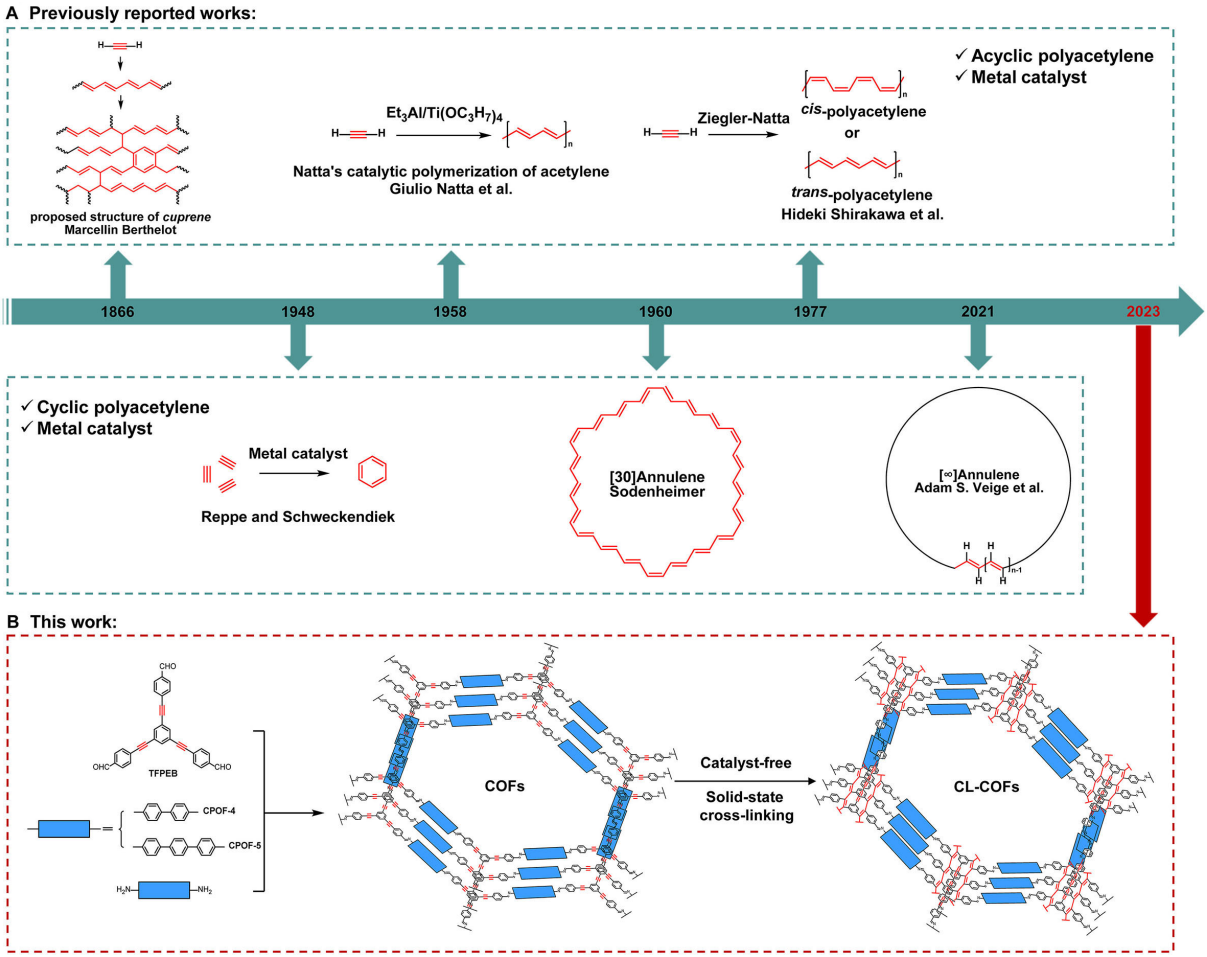

Scheme 1. Historical development of acetylenic polymers. (A) Previously reported acetylenic polymers and corresponding structures; (B) This study presents the synthesis of 2D COFs and the proposed mechanism of transforming them into crystalline CL-COFs via solid-state cross-linking in confined spaces. COFs: Covalent organic frameworks; CL-COFs: crystalline cross-linked covalent organic frameworks.

distance. This model of stacking provides the possibility for thermally induced layer-to-layer cross-linking, while only negligible changes in the framework occur. In addition, the CL-COFs formed after cross-linking have higher electronic conductivity than the pristine COFs.

EXPERIMENTAL

Materials and chemicals

All chemicals and solvents were purchased from commercial suppliers. Specifically, 4,4′-diaminobiphenyl (DABP) and 4,4″-diamino-p-terphenyl (DATP) were purchased from Aladdin®. Additionally, 1,2-dichlorobenzene (*o*-DCB), *N*,*N*-dimethylacetamide (DMAc), and diphenyl sulfone were obtained from J&K Scientific LTD. Acetic acid and organic solvents, including dichloromethane (DCM), *n*-hexane, acetone, and tetrahydrofuran (THF), were purchased from Xilong Scientific. All reagents and solvents were used without further purification unless otherwise specified.

Synthesis of 1,3,5-tri(4-formylphenylethynyl)benzene

Under a nitrogen atmosphere, 1,3,5-triethynylbenzene (1.2 g, 8.0 mmol, 1.0 eq.), 4-iodobenzaldehyde (5.6 g, 24.0 mmol, 3.0 eq.), dichlorobis(triphenylphosphine)palladium(II) (0.34 g, 0.48 mmol, 0.02 eq.) were

dissolved in 200 mL of anhydrous THF. Dry triethylamine (8.0 mL, 57 mmol) was added, and the mixture was stirred for 10 min; then, the catalyst copper(I) iodide (0.19 g, 1.0 mmol, 0.04 eq.) was added, turning the solution to dark brown. After stirring for 16 h at room temperature, the solvent was evaporated at reduced pressure, and the resulting solid mixture was washed with brine-saturated solution of NH_4Cl and extracted with DCM. The purification was made by column chromatography on silica gel using DCM as eluent to afford the desired product as a colorless solid (2.18 g, Yield: 59%); ^{1}H NMR (400 MHz, $CDCl_3$): δ_H 10.04 (s, 3H), 7.90 (d, J = 8.3 Hz, 6H), 7.74 (s, 3H), 7.69 (d, J = 8.2 Hz, 6H); ^{13}C NMR (101 MHz, $CDCl_3$): δ_C 191.5, 136.0, 135.0, 132.4, 129.8, 128.9, 123.8, 91.3, 90.1.

Preparation of CPOF-4

A Pyrex tube measuring o.d. × i.d. = 10 × 8 mm^2 was charged with 1,3,5-tri(4-formylphenylethynyl)benzene (TFPEB) (13.9 mg, 0.03 mmol), DABP (8.3 mg, 0.045 mmol) in a mixed solution of *o*-DCB (0.5 mL), DMAc (0.5 mL), and 6.0 M acetic acid (0.1 mL). The Pyrex tube was flash frozen in a liquid nitrogen bath sealed under vacuum. Upon warming to room temperature, the tube was placed in an oven at 120 °C for three days. The yellow solid was isolated by filtration and washed with THF (3 × 15 mL), acetone (3 × 15 mL), and *n*-hexane (3 × 15 mL). The powder was dried at 80 °C under vacuum overnight to afford the CPOF-4 as a yellow crystalline solid (15.4 mg, Yield: 75%).

Synthesis and activation of CPOF-4-265 °C-*X* h (*X* = 12, 48 and 84)

For example, a 5 mL vial charged with CPOF-4 (100.0 mg) and diphenyl sulfone (3 g), The vial was then transferred to a tubular furnace and evacuated, filled with N_2 by five cycles. Subsequently, the temperature was raised to 265 °C at the rate of 10 °C·min^{-1} in a N_2 flowing atmosphere with a flow rate of 20 mL·min^{-1}. After heating at 265 °C for a certain period of time, the temperature was reduced to room temperature at the rate of 10 °C·min^{-1}. Finally, the obtained product was washed with THF and acetone to remove the residual diphenyl sulfone and dried at 120 °C under vacuum overnight to afford the CPOF-4-265 °C-*X* h (*X* = 12, 48 and 84) as a brown black crystalline solid. Similarly, the thermally cross-linked products of CPOF-5 are named CPOF-5-265 °C-*X* h (*X* = 48 and 84).

Characterizations

^{1}H NMR spectra were measured on a Bruker Fourier 400 MHz spectrometer. Solid-state NMR spectra were recorded at ambient pressure on a Bruker Fourier 600 MHz spectrometer using a standard CP pulse sequence probe with 3.2 mm (outside diameter) zirconia rotors. The Fourier-transform infrared (FT-IR) spectra (KBr) were obtained using a SHIMADZU IRAffinity-1 FT-IR spectrophotometer. A SHIMADZU UV-2450 spectrophotometer was used for all absorbance measurements. Powder X-ray diffraction (PXRD) patterns were carried out in a reflection mode on a Bruker D8 advance powder diffractometer with Cu Kα (λ = 1.5418 Å) line focused radiation at 40 kV and 40 mA from 2^θ = 1.0° up to 40° with 0.020481 increment by Bragg-Brentano. The powdered sample was added to the glass and compacted for measurement. Thermogravimetric analysis (TGA) was recorded on a SHIMADZU DTG-60 thermal analyzer under N_2. The operational range of the instrument was from 30 to 800 °C at a heating rate of 10 °C·min^{-1} with a N_2 flow rate of 30 mL·min^{-1}. Raman spectra were recorded on a Renishaw in a Via-Reflex confocal Raman microscope with an excitation wavelength of 325 nm. X-ray photoelectron spectroscopy (XPS) was obtained on an ESCALAB 250 spectrophotometer with Al-Kα radiation. The binding energy (BE) values were referred to as the C single bond (C, H) contribution of the C 1s peak fixed at 284.8 eV. Electron paramagnetic resonance (EPR) spectra are recorded on a Bruker EMXplus-10/12 spectrometer under room temperature. The microwave frequency was 9.8 GHz, and the modulation amplitude microwave power was about 2 mW. The adsorption-desorption isotherms of N_2 were obtained at 77 K using a BELSORP MAX gas sorption analyzer. Before sorption analysis, the sample was evacuated at 100 °C for 12 h using a turbomolecular vacuum pump. Specific surface areas were calculated from N_2 adsorption data by multipoint

BET analysis. Quenched solid density functional theory (QS-DFT) was applied to analyze the N_2 isotherm based on the model of N_2@77 K on carbon with cylindrical pores. Scanning electron microscopy (SEM) was performed on a Zeiss Gemini SEM 300 microscope instrument. Samples were prepared by dispersing the material onto conductive adhesive tapes attached to a flat aluminum sample holder and then coated with gold. High resolution transmission electron microscope (HR-TEM) analysis was collected on a JEOL JEM-2100 microscope instrument at 200 kV. A synthesized sample was dispersed into ethyl alcohol to obtain a highly dispersed suspension. Then, one droplet was transferred onto a carbon film-supported TEM grid.

Electrical conductivity measurements.

Electrochemistry experiments were conducted on a CHI660C Electrochemical Workstation (Shanghai ChenHua Electrochemical Instrument). The obtained powder was ground before being added into a 0.5-cm die. Then, the die pressure was slowly increased to 4.0 MPa and kept for 1 h to prepare pellets (diameter = 0.5 cm, thickness = 0.5 cm). Two pieces of gold (diameter = 0.5 cm) with wires are attached to both sides of the pellet. The current-voltage (I-V) measurement was performed in conditions by sweeping the voltage from -1.0 to 1.0 V. The obtained conductivity was collected at 25 °C in a N_2 atmosphere.

RESULTS AND DISCUSSION

Our strategic preparation of 2D COFs is based on condensation of triangular building block, TFPEB, and amino-based linear linkers of different lengths, DABP or DATP, that resulted in two novel acetylenic group bridged 2D COFs, namely, CPOF-4, and CPOF-5 (CPOF = crystalline porous organic framework), respectively. After this, solid-state cross-linking of COFs was carried out at 265 °C, and the addition of diphenyl sulfone was targeted to make COFs heated uniformly at high temperatures. In order to verify the cross-linking reaction of acetylenic groups between COF layers to form polyacetylene structures, the CL-COFs were characterized by FT-IR and solid-state ^{13}C NMR spectroscopy. The FT-IR spectrum exhibited a new peak at 1,623 cm^{-1} for CPOF-4 or 1,622 cm^{-1} for CPOF-5, which is a typical stretching vibration of the C=N bond, confirming the transformation of the aldehyde and amine groups. The peak at 2,206 cm^{-1} for CPOF-4 or 2,207 cm^{-1} for CPOF-5 can be attributed to the formation of C≡C bonds [Supplementary Figures 1 and 2]. By testing the *in-situ* variable-temperature infrared spectra (IR) of CPOF-4 at 215, 265, and 295 °C, we found that the acetylenic groups in 2D COFs barely react at 215 °C, slowly cross-link at 265 °C, and react violently at 295 °C [Supplementary Figures 3-6]. In order to avoid the formation of unnecessary by-products at high temperatures, we opted to perform the solid-state cross-linking of 2D COFs at 265 °C. After several days of heating, the FT-IR spectrum clearly exhibited that the absorption peak of the C≡C bonds weakened, indicating the occurrence of cross-linking [Figure 1A and Supplementary Figure 7]. ^{13}C NMR results showed that the absorption peak of 137-140 ppm was broadened after 265 °C heating [Figure 1B, Supplementary Figures 8 and 9], further proving that cross-linking forms a *trans*-polyacetylene structure[34-36]. Furthermore, after 84 h of heating, the reaction conversions calculated from the peak areas of C≡C bonds of CPOF-4 and CPOF-5 were both close to 60%~70%. The results clearly showed that the acetylenic groups inside the COFs are successfully cross-linked without a catalyst.

In order to evaluate the composition of the products after the cross-linking reaction of 2D COFs, we performed detailed hydrolysis experiments on CPOF-4-265 °C-84 h samples [Supplementary Figures 10 and 11]. The synthetic details have been described in Sections S13-20 (Supplementary Materials). From the energy dispersive spectrometer (EDS) analysis results, it can be seen that the residual insoluble solid after hydrolysis does not contain elemental N [Supplementary Figures 12 and 13], and the liquid ^{1}H NMR reveals that DABP monomer is produced [Supplementary Figure 14]. Therefore, it can be determined that the N-containing part of the original structure is completely transformed into soluble DABP monomer. We also

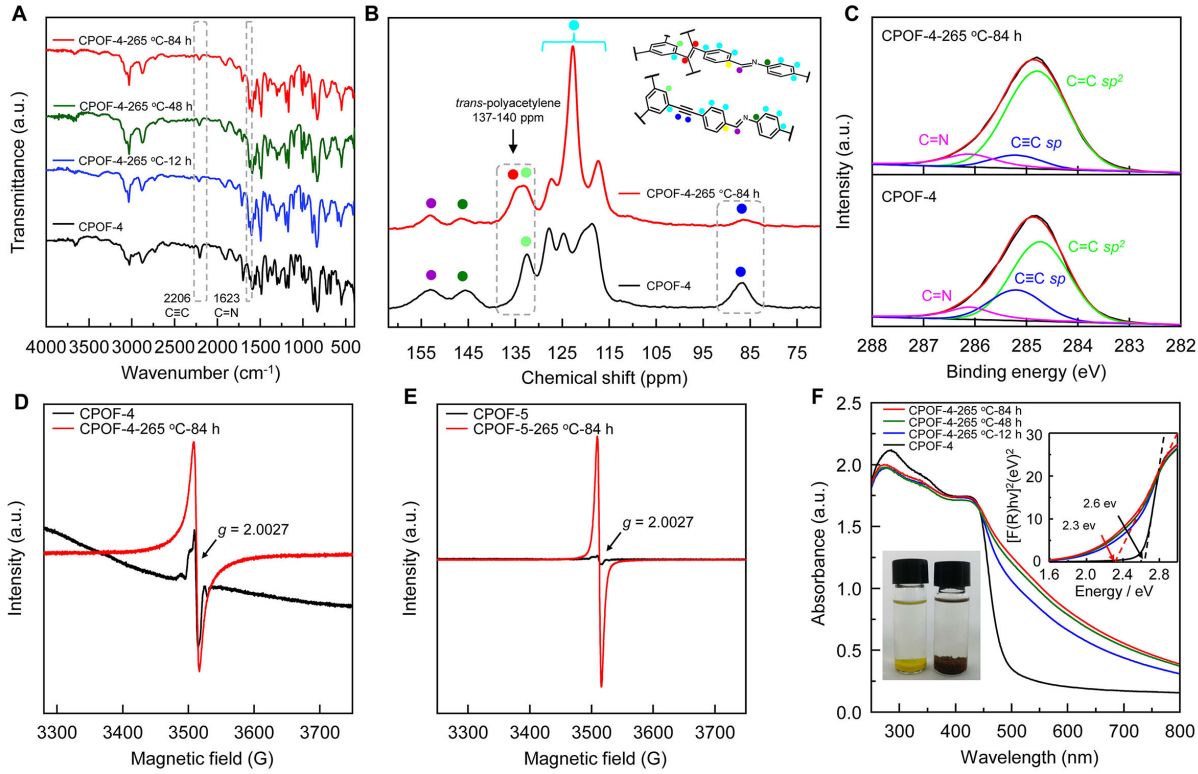

Figure 1. (A) FT-IR spectra analyses of CPOF-4-265 °C-*X* h (*X* = 12, 48 and 84) compared with the CPOF-4; (B) ^{13}C CP-MAS NMR spectra of CPOF-4 and CPOF-4-265 °C-84 h; (C) High-resolution C 1s XPS peak of CPOF-4 (down) and CPOF-4-265 °C-84 h (top); (D) Solid-state EPR spectrum of CPOF-4 (black) and CPOF-4-265 °C-84 h (red); (E) Solid-state EPR spectrum of CPOF-5 (black) and CPOF-5-265 °C-84 h (red); (F) UV-vis DRS of CPOF-4 and CPOF-4-265 °C-*X* h (*X* = 12, 48 and 84). Inset: CPOF-4 (left) and CPOF-4-265 °C-84 h (right) immersed in THF. FT-IR: Fourier-transform infrared; EPR: electron paramagnetic resonance; DRS: diffuse reflection spectroscopy; THF: tetrahydrofuran.

noticed that a small amount of TFPEB monomer was released after hydrolysis due to incomplete cross-linking of the acetylene groups, which resulted in the yield of insoluble solids lower than the theoretical value. Impressively, the ^{13}C NMR spectra of acid-digested CPOF-4-265 °C-84 h showed a very sharp characteristic peak of *trans*-polyacetylene at 137 ppm [Supplementary Figure 15]. Raman spectroscopy is an effective analytical method for demonstrating the formation of polyacetylene structures. From the Raman characterization of acid-digested CPOF-4-265 °C-84 h, it can be seen that peaks at 1,583 and 1,370 cm^{-1} can be assigned to in-phase C=C stretching and C–C stretching vibrations of the *trans*-polyacetylene structure, respectively[37-40]. Additionally, the lower frequency mode at 1,100 cm^{-1} is mainly due to the C–H in-plane bending modes in the benzene ring. Raman spectra further clarified that the formed *trans*-polyacetylene structure in CPOF-4-265 °C-84 h [Supplementary Figure 16]. Interestingly, the gas adsorption test results show that acid-digested CPOF-4-265 °C-84 h hardly adsorbs N_2 but has a good adsorption capacity for CO_2 [Supplementary Figures 17-23]. These phenomena, coupled with selective adsorption, can be attributed to the narrow window in acid-digested CPOF-4-265 °C-84 h[41].

The chemical compositions and elemental chemical states of COFs and CL-COFs were further investigated by XPS. The XPS general survey of the synthesized powder indicated mainly the presence of C, O, and N without any detectable S contaminants. The presence of O 1s peak is ascribed to the adsorption of air in the pores [Supplementary Figures 24 and 25]. The high-resolution C 1s XPS spectra of the CPOF-4 exhibited three characteristic peaks at 284.7, 285.2, and 286.1 eV [Figure 1C, Supplementary Figures 26 and 27], which

are attributed to the C=C (sp^2), C≡C (sp), and C=N bonds, respectively[42-44]. Based on analysis of the characteristic peak intensity of the CPOF-4 and CPOF-4-265 °C-84 h, the C 1s XPS spectra of CPOF-4-265 °C-84 h showed that the peak area for C≡C decreases obviously as compared to CPOF-4. Meanwhile, the peak area of C=C increases visibly, but that of C=N remains unchanged. The area ratio of the sp^2 and the sp subpeaks is about 3.3 in CPOF-4 and 10.4 in CPOF-4-265 °C-84 h [Supplementary Table 1], indicating that about 62% of the C≡C was converted to C=C, which is consistent with the ^{13}C NMR results. Meanwhile, the XPS characterization results revealed that the reaction conversion of acetylene groups in CPOF-5 is similar to that of CPOF-4 (details in Sections S21-23, Supplementary Materials). The results clearly showed that the acetylenic groups inside the COFs are successfully cross-linked without a catalyst.

One of the remarkable features of *trans*-polyacetylene is its intrinsic neutral soliton defects (bond alternation domain walls) with spin properties[45-48], and the magnetic moments of solitons can be detected by EPR. Here, we performed EPR characterization on these samples. As shown in Figure 1D and E, the pristine 2D COFs showed a very weak EPR signal, which may originate from unreacted terminal amino or aldehyde groups at the boundaries of 2D layered crystals[49]. Impressively, the EPR spectral intensities of CPOF-4-265 °C-84 h and CPOF-5-265 °C-84 h are significantly enhanced, and the narrow Lorentzian line shapes signal with g = 2.0027 can be attributed to neutral soliton defects inherent in the *trans*-polyacetylene structure. Moreover, the EPR signal intensity of the CPOF-4-265 °C-84 h can be further enhanced after iodine doping, which indicated the generation of more charge carriers as pairs of radicals and cations [Supplementary Figures 28-31][50,51]. Thus, these results fully demonstrate the formation of polarons in CPOF-4-265 °C-84 h and CPOF-5-265 °C-84 h.

Comparing the UV-vis spectra of CPOF-4 and CPOF-5 at different reaction times, it can be seen that the absorption range of the corresponding products is gradually broadened, and the absorption sideband gradually redshifts as the reaction time is prolonged, indicating that the internal conjugate system of the material increases. More interestingly, the analysis of the Tauc plot reveals that this solid-state cross-linking of acetylenic groups in confined space can effectively adjust the optical band gaps (E_g) of the material [Figure 1F and Supplementary Figure 32]. It can be clearly seen that the band gap gradually decreases from the initial ~2.6 to ~2.3 eV for CPOF-4 and from ~2.6 to ~2.4 eV for CPOF-5. Moreover, the frontier orbitals of CPOF-4 and CPOF-4-265 °C-84 h were calculated using density functional theory calculations (DFT). The results showed that after solid-state cross-linking, the energy gap decreases from ~2.1 to ~1.3 eV due to the formation of interlayer polyacetylene conjugated structures [Supplementary Figures 33 and 34], indicating that the framework has higher charge transfer and separation capabilities (details in Section S27, Supplementary Materials).

We also directly polymerized the monomer containing acetylenic groups by heating, denoted as the polymer-model. FT-IR analysis showed that the absorption peak of acetylene at 2,208 cm^{-1} was obviously weakened [Supplementary Figures 35 and 36], indicating that the monomer could be successfully polymerized. The nitrogen adsorption isotherm at 77 K revealed the microporous nature of the polymer-model and yielded a BET surface area of 297 $m^2 \cdot g^{-1}$ [Supplementary Figures 37-39]. However, experimental PXRD patterns showcased the amorphous nature of the polymer-model [Supplementary Figure 40]. These results further demonstrate that the solid-state cross-linking under framework constraints can effectively preserve the crystal structure of the material.

The crystalline structures of as-synthesized 2D COFs and CL-COFs were assessed by PXRD analyses. The experimental PXRD patterns exhibited strong diffraction peaks at 2θ = 1.9°, 3.3°, 3.9°, and 5.1° for CPOF-4

and 1.7°, 2.9°, 3.4°, and 4.6° for CPOF-5 corresponding to the (100), (110), (200), and (220) facets, respectively. After a geometrical energy minimization by using the Materials Studio software package based on the 2D **hcb** topology with AA stacking modes, the unit cell parameters were obtained [Supplementary Figures 41 and 42]. Moreover, full profile pattern matching (Pawley) refinements were applied to their experimental PXRD patterns, and the refinement results yielded unit cell parameters nearly equivalent to the simulations with good agreement factors (CPOF-4: $a = b = 53.87$ Å, $c = 3.47$ Å, $\alpha = \beta = 90°$, $\gamma = 120°$, $R_{wp} = 4.74\%$ and $R_p = 3.12\%$; CPOF-5: $a = b = 61.49$ Å, $c = 3.48$ Å; $\alpha = \beta = 90°$, $\gamma = 120°$, $R_{wp} = 8.74\%$ and $R_p = 6.68\%$) [Figure 2A and Supplementary Figure 43]. After heating-induced cross-linking, the (hk0) diffraction peaks of CL-COFs exhibited stronger diffraction intensity and narrower half-peak width, which indicates that the crystallinity of the material was enhanced. This is due to the cross-linking effect limiting the interlayer slip of 2D COFs, which makes the stacking between layers more strict [Supplementary Table 2]. On the other hand, the diffraction peak shifted slightly to higher angles with increasing heating time, to $2\theta = 2.0°$, 3.5°, 4.1°, and 5.4° for CPOF-4 and 1.8°, 3.1°, and 3.7° for CPOF-5 after reaction for 84 h [Figure 2B, Supplementary Figures 44 and 45]. This is due to the covalent bond between the lower layer and the layer induced by high temperature, which endows the initial planar structure with a certain orientation in the vertical direction[30-33]. The crystal structures of CPOF-4-265 °C-84 h and CPOF-5-265 °C-84 h were constructed by directly connecting acetylene groups between adjacent layers along the crystallographic *c*-axis direction of 2D COFs, and structure optimization was performed. The refinement results can match well with the observed ones with good agreement factors (CPOF-4-265 °C-84 h: $a = 50.99$ Å, $b = 50.90$ Å, $c = 5.24$ Å, $\alpha = 90.0°$, $\beta = 90.4°$, $\gamma = 119.9°$, $R_{wp} = 5.47\%$ and $R_p = 3.65\%$; CPOF-5-265 °C-84 h: $a = 58.37$ Å, $b = 58.34$ Å, $c = 5.30$ Å, $\alpha = 89.9°$, $\beta = 89.9°$, $\gamma = 120.2°$, $R_{wp} = 5.94\%$ and $R_p = 4.44\%$) [Figure 2C-E, Supplementary Figures 46-49].

The effect of cross-linking reaction on porosity and textural properties was evaluated by N_2 adsorption-desorption measurements at 77 K. The adsorption isotherms of these 2D COFs belong to the typical type-IV isotherm that reveals the characteristics of mesoporous materials [Figure 2F, Supplementary Figures 54-67]. Specifically, the desorption branch of CPOF-4 and CPOF-5 isotherms is found to be higher than the adsorption branch at lower relative pressure, which suggests swelling effect of the framework[52,53]. Meanwhile, the desorption branches of CPOF-4-265 °C-84 h and CPOF-5-265 °C-84 h completely overlap with the adsorption branches, indicating that the frameworks become rigid and stable after layer-to-layer cross-linking. The BET surface areas calculated from the N_2 adsorption results were found to be 447 and 157 $m^2 \cdot g^{-1}$ for CPOF-4 and CPOF-5, respectively. Interestingly, the BET surface area increased significantly after heating at 265 °C for 84 h, yielding 2,137 and 1,363 $m^2 \cdot g^{-1}$ for CPOF-4 and CPOF-5, corresponding to five-fold and nine-fold increments, respectively. Specifically, the adsorption isotherms of these CL-COFs exhibited a rapid N_2 uptake at a low relative pressure range ($P/P_0 < 0.05$), indicative of the N_2 molecules feeding into the honeycomb pores rapidly. Meanwhile, a sharp step between $P/P_0 = 0.2$ and 0.4 was observed, which is characteristic of mesoporous materials. The pore size distribution of 2D COFs based on the QS-DFT using cylindrical pore models demonstrated mesopore widths (4.4 nm for CPOF-4 and 4.9 nm for CPOF-5), which is in good agreement with the simulated pore sizes. After cross-linking reaction, the pore widths showed a slight decrease (4.1 nm for CPOF-4-265 °C-84 h and 4.5 nm for CPOF-5-265 °C-84 h. These results were consistent with PXRD profiles that showed a slight shift towards higher angles.

The morphologies of both 2D COFs are ascertained by SEM and TEM. SEM inspection revealed a sheet-like morphology of the CPOF-4 and CPOF-5 [Supplementary Figures 68 and 69], and the morphology of the corresponding CPOF-4-265 °C-84 h and CPOF-5-265 °C-84 h formed after cross-linking remained nearly identical [Supplementary Figures 70 and 71]. Furthermore, the crystalline structures of these materials were confirmed by high-resolution TEM (HR-TEM) but only for CPOF-4-265 °C-84 h and CPOF-5-265 °C-84 h

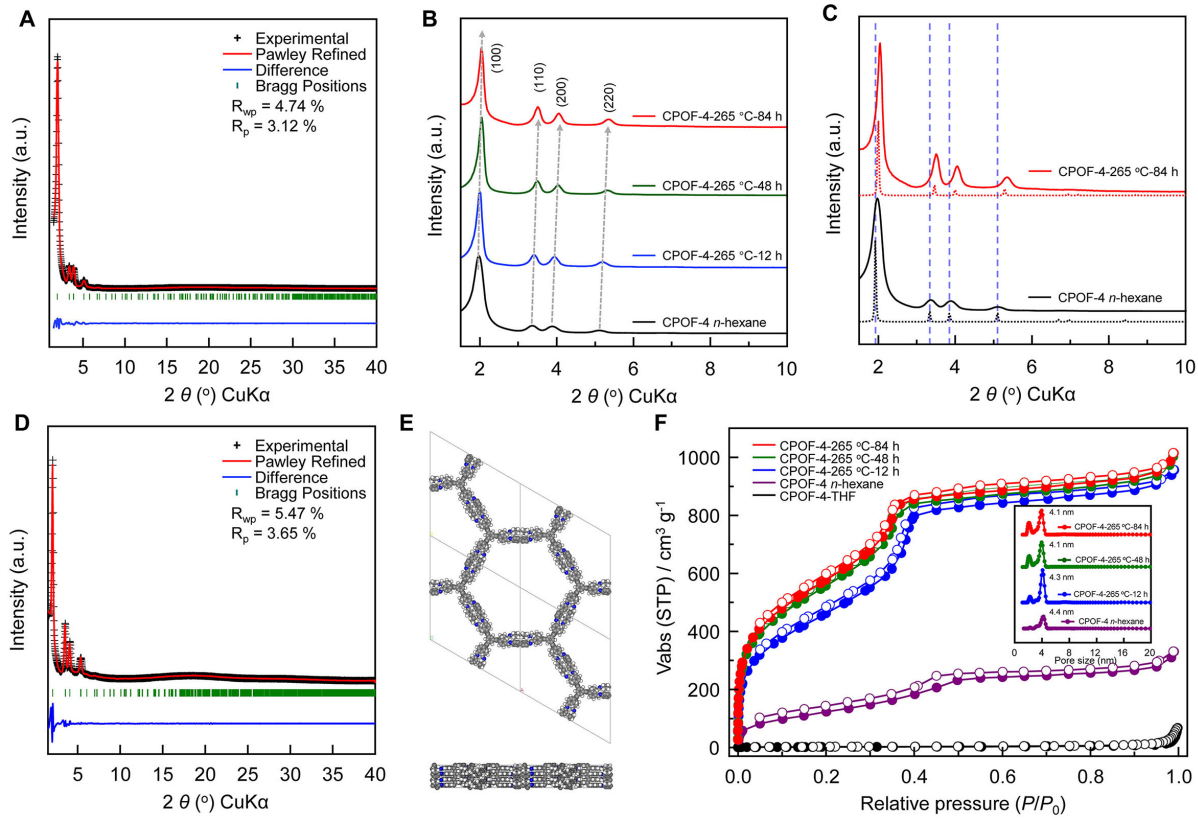

Figure 2. (A) PXRD patterns of CPOF-4: comparison between the experimental (black) and Pawley refined (red) profiles, the refinement differences (blue), and the Bragg positions (green); (B) PXRD pattern analyses of CPOF-4-265 °C-*X* h (*X* = 12, 48, and 84) compared with the CPOF-4; (C) PXRD patterns of CPOF-4 and CPOF-4-265 °C-84 h: experimentally observed (solid line) and simulated based on eclipsed stacking modes (dashed line); (D) PXRD patterns of CPOF-4-265 °C-84 h: comparison between the experimental (black) and Pawley refined (red) profiles, the refinement differences (blue), and the Bragg positions (green); (E) Space-filling models of CPOF-4-265 °C-84 h. Carbon, gray; Nitrogen, blue; Hydrogen, white; (F) N_2 adsorption/desorption isotherms of CPOF-4 and CPOF-4-265 °C-*X* h (*X* = 12, 48 and 84). PXRD: Powder X-ray diffraction.

because CPOF-4 and CPOF-5 were found to be extremely unstable under the electron beam, and thus, their HR-TEM could not be obtained[54,55]. In sharp contrast, the HR-TEM images of CPOF-4-265 °C-84 h and CPOF-5-265 °C-84 h taken along the [001] direction revealed an ordered, honeycomb-like porous structure with a periodicity of 4.1 ± 0.2 nm for CPOF-4-265 °C-84 h and 4.8 ± 0.1 nm for CPOF-5-265 °C-84 h, respectively [Supplementary Figures 72-75]. The observed results are consistent with the pore-to-pore distance between the pores in the simulated structures.

The thermal stabilities of the 2D COFs were evaluated by TGA. The two 2D COFs showed barely noticeable skeleton weight loss before 440 °C [Supplementary Figures 76 and 77]. In order to evaluate the effect of solid-state cross-linking on the chemical stability of the materials, the 2D COFs and CL-COFs were immersed in different solvents, including *n*-pentane, *n*-hexane, DCM, acetone, THF, MeOH, DMF, boiling water, concentrated NaOH (10 M), and concentrated HCl (1 M), for 24 h. PXRD results showed that both 2D COFs lost their crystallinity after being activated in DCM, acetone, THF, MeOH, and DMF but maintained high crystallinity in *n*-hexane and *n*-pentane [Figure 3 and Supplementary Figures 78-81]. This might originate from the acetylenic groups (–C≡C–) into a 2D COF framework, resulting in very weak van der Waals interactions, which do not contribute to interlayer packing of the 2D polymers and lead to very low crystallinity[56,57]. The weak π–π interaction between 2D COF adjacent layers fails to counteract the

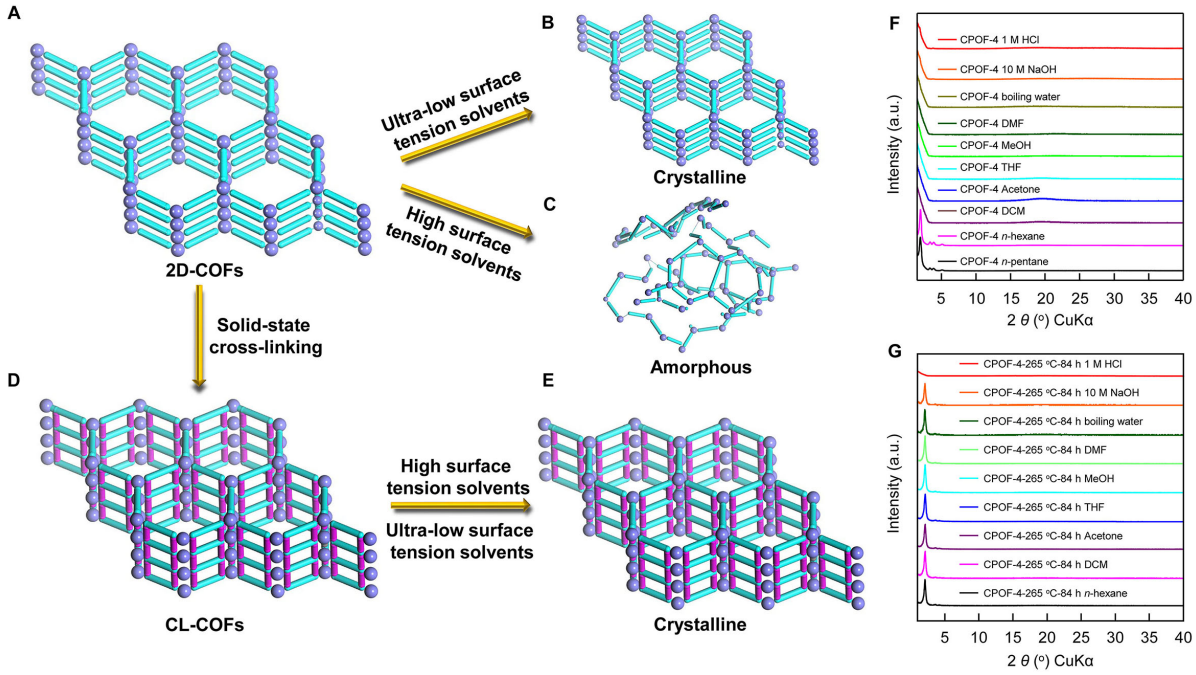

Figure 3. Stability test of 2D COFs and CPOF-4-265 °C-84 h. Effect of solvent activation on (A-C) 2D COF structure and (D and E) CL-COF structure; (F) PXRD patterns of CPOF-4 after solvent treatments under different chemical environments for 24 h; (G) PXRD patterns of CPOF-4-265 °C-84 h after treatments under different chemical environments for 24 h. COFs: Covalent organic frameworks; CL-COF: crystalline cross-linked covalent organic framework; PXRD: powder X-ray diffraction.

strong surface tension and capillary forces generated during liquid-gas phase transition of the guest molecules with high surface tension, thereby resulting in framework collapse[58,59]. In addition, both 2D COFs are also found to be unstable in the harsh environments of concentrated acid/base/boiling water. N_2 adsorption isotherm tests showed consistent results, such as the activation of CPOF-4 when performed using THF, resulted in a very low BET surface area, whereas activation with ultra-low surface tension solvent *n*-hexane yielded a high surface area. In sharp contrast, CPOF-4-265 °C-84 h and CPOF-5-265 °C-84 h maintained their original crystalline structure after solvent treatment under the above chemical environments except under strong acidic conditions. This result further confirms that the covalent bonds formed by the cross-linking between the layers endow the framework with sufficient rigidity to overcome the framework collapse caused by the solvent activation process.

The high surface areas and stability of CL-COFs inspired us to investigate the solid-state cross-linking reaction characteristics of acetylenic groups in 2D COFs, which will help to identify more suitable reaction conditions to construct CL-COFs. Since reaction temperature can strongly influence the morphology of the polyacetylene with consequences in its quality, isomeric content, crystallinity, and conductivity[60,61], we performed *in-situ* FT-IR studies of 2D COFs at 215, 265, and 295 °C, respectively [Supplementary Figure 82]. It should be emphasized that the absorbance of a substance (here, we use the peak area to represent it) is proportional to the concentration, so the change of the acetylenic group peak area can indicate its concentration change in the solid-state cross-linked system of 2D COFs. The results showed that the reaction rate started fast and decreased after about 2 h. The reaction at 265 and 295 °C could be divided into two stages: a fast stage and a slow stage. This reaction feature has also been reported in the previous literature[62,63]. Furthermore, in the slow reaction stage, the absorption peak area of the acetylene group is proportional to time, indicating that the zero-order model can describe the reaction

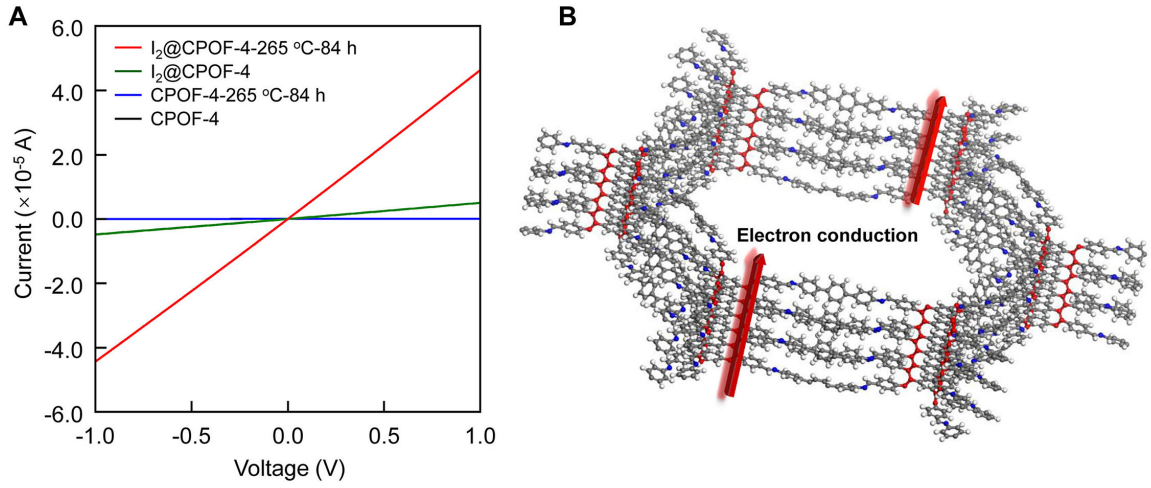

Figure 4. Study of electron conduction. (A) I-V curves of CPOF-4 and CPOF-4-265 °C-84 h upon I_2 oxidation; (B) Schematic representation of electron conduction in CPOF-4-265 °C-84 h. I-V: Current-voltage.

kinetic characteristics of the acetylenic groups. The rate constant *k* values at each reaction temperature obtained from the slope of each straight line are listed in Supplementary Table 3. As the temperature rose, the reaction rate constant exponentially increased. To obtain thermodynamic parameters, the activation energy of the reaction was calculated using the Arrhenius formula. Therefore, the activation energy can be calculated to be 88.5 kJ·mol^{-1} [Supplementary Figure 83].

Doped polyacetylene, as an emerging kind of conjugated conducting polymer, demonstrates a substantial increase in conductivity upon doping with halogens[64,65]. Inspired by this, we evaluated the I-V characteristics (I-V curves) of CPOF-4 and CPOF-4-265 °C-84 h after iodine doping to understand the influence of solid-state cross-linking on the conductivity of the material. The I_2@CPOF-4 and I_2@CPOF-4-265 °C-84 h were synthesized by exposing the powdered samples to I_2 vapor at 75 °C for 24 h. As shown in Figure 4, both CPOF-4 and CPOF-4-265 °C-84 h showed insulating behavior before I_2 doping. The conductivity of the I_2@CPOF-4 was measured to be 1.3 × 10^{-5} S·cm^{-1}. Notably, I_2@CPOF-4-265 °C-84 h showed a marked ten-fold enhancement in conductivity, reaching 1.2 × 10^{-4} S·cm^{-1}. The significant enhancement in conductivity of CPOF-4-265 °C-84 h from that of 2D COFs is mainly attributed to the conjugated polyacetylene structure of the former, which exhibits high conductivity after doping with charge carriers (details in Section S57, Supplementary Materials). Nevertheless, the conductivity of I_2@CPOF-4-265 °C-84 h cannot be compared with classical polyacetylene. We speculate that this may be due to the incomplete cross-linking reaction of acetylene groups leading to low conjugation of the structure of CPOF-4-265 °C-84 h, which has a relatively large band gap and low electrical conductivity[66].

CONCLUSIONS

In conclusion, we have succeeded in developing the first case of exploiting acetylene (–C≡C–) as a reaction site to achieve solid-state cross-linking of acetylene (–C≡C–) within the confined space of the framework under thermal induction, thereby constructing crystalline CL-COFs. This strategy realizes the synthesis of polyacetylene without a catalyst and improves the crystallinity, specific surface area, and stability of the material. Furthermore, the conductivity of the material was markedly improved by doping I_2. This study will open new vistas for exploiting nanoconfined spaces of reticular frameworks, facilitating a paradigm shift from solution polymerizations into solid-state cross-linking.

DECLARATIONS

Authors' contributions

Conducted the preparation and characterization of COFs and prepared the draft manuscript: Zhao Y, Wen D
Performed the *in-situ* Fourier-transform infrared (FT-IR) characterization: Fu J
Collected and analyzed the nuclear magnetic resonance spectroscopy data: Das S
Performed the transmission electron microscopy (TEM) characterization: Wang Y, Zhao Z
Conducted the density functional theory (DFT) calculation: Qiao Z, Gao Y, Cao D, Peng D
Planned the study, analyzed the data, and wrote the manuscript: Zhu W, Ben T

Availability of data and materials

Not applicable.

Financial support and sponsorship

This work was supported by the National Key R&D Program of China (2021YFA1200400), the National Natural Science Foundation of China (Nos. 91956108 and 22201256), and the Natural Science Foundation of Zhejiang Province (No. LZ22B010001).

Conflicts of interest

All authors declared that there are no conflicts of interest.

Ethical approval and consent to participate

Not applicable.

Consent for publication

Not applicable.

REFERENCES

1. Shirakawa H, Louis EJ, Macdiarmid AG, Chiang CK, Heeger AJ. Synthesis of electrically conducting organic polymers: halogen derivatives of polyacetylene, (CH)*x*. *J Chem Soc Chem Commun* 1977:578-80. DOI
2. Chiang CK, Fincher Jr CR, Park YW, et al. Electrical conductivity in doped polyacetylene. *Phys Rev Lett* 1977;39:1098-101. DOI
3. Shirakawa H. The discovery of polyacetylene film: the dawning of an era of conducting polymers (Nobel lecture). *Angew Chem Int Ed* 2001;40:2574-80. DOI PubMed
4. Heeger AJ. Nobel lecture: semiconducting and metallic polymers: the fourth generation of polymeric materials. *Rev Mod Phys* 2001;73:681. DOI
5. Chiang CK, Druy MA, Gau SC, et al. Synthesis of highly conducting films of derivatives of polyacetylene, (CH)*x*. *J Am Chem Soc* 1978;100:1013-5. DOI
6. Rasmussen SC. Conjugated and conducting organic polymers: the first 150 years. *Chempluschem* 2020;85:1412-29. DOI PubMed
7. Flory PJ. The heat of combustion and structure of cuprene. *J Am Chem Soc* 1937;59:1149-50. DOI
8. Rasmussen SC. Cuprene: a historical curiosity along the path to polyacetylene. *Bull Hist Chem* 2017;42:63-78. Available from: http://acshist.scs.illinois.edu/awards/OPA%20Papers/2018-Rasmussen.pdf. [Last accessed on 10 Jan 2024]
9. Natta G, Mazzanti G, Corradini P. Stereospecific polymerization of acetylene. *Atti Accad Naz Lincei Cl Sci Fis Mat Nat Rend* 1958;25:3-12. (in German). Available from: https://www.giulionatta.it/pdf/pubblicazioni/00296.pdf. [Last accessed on 10 Jan 2024]
10. Reppe W, Schweckendiek WJ. Cyclizing polymerization of acetylene. III Benzene, benzene derivatives and hydroaromatic compounds. *Justus Liebigs Ann Chem* 1948;560:104-16. Available from: https://chemistry-europe.onlinelibrary.wiley.com/doi/10.1002/jlac.19485600104. [Last accessed on 12 Jan 2024]
11. Sondheimer F, Wolovsky R. The synthesis of cycloöctadecanonaene, a new aromatic system. *Tetrahedron Lett* 1959;1:3-6. DOI
12. Sondheimer F, Gaoni Y. Unsaturated macrocyclic compounds. XV.[1] Cyclotetradecaheptaene. *J Am Chem Soc* 1960;82:5765-6. DOI
13. Miao Z, Gonsales SA, Ehm C, et al. Cyclic polyacetylene. *Nat Chem* 2021;13:792-9. DOI PubMed PMC

14. Foster JC, O'Reilly RK. How to better control polymer chemistry. *Science* 2019;363:1394. DOI PubMed
15. Biradha K, Santra R. Crystal engineering of topochemical solid state reactions. *Chem Soc Rev* 2013;42:950-67. DOI PubMed
16. Grommet AB, Feller M, Klajn R. Chemical reactivity under nanoconfinement. *Nat Nanotechnol* 2020;15:256-71. DOI
17. Fu Q, Bao X. Surface chemistry and catalysis confined under two-dimensional materials. *Chem Soc Rev* 2017;46:1842-74. DOI PubMed
18. Chen Z, Guan B, Chen X, et al. Fast and uniform growth of graphene glass using confined-flow chemical vapor deposition and its unique applications. *Nano Res* 2016;9:3048-55. DOI
19. Wegner G. Solid-state polymerization mechanisms. *Pure Appl Chem* 1977;49:443-54. DOI
20. Tanaka K, Toda F. Organic photoreaction in the solid state. In: Toda F, editor. Organic solid-state reactions. Dordrecht: Springer; 2002. pp. 109-58. DOI
21. Côté AP, Benin AI, Ockwig NW, O'Keeffe M, Matzger AJ, Yaghi OM. Porous, crystalline, covalent organic frameworks. *Science* 2005;310:1166-70. DOI PubMed
22. Diercks CS, Yaghi OM. The atom, the molecule, and the covalent organic framework. *Science* 2017;355:eaal1585. DOI PubMed
23. Colson JW, Dichtel WR. Rationally synthesized two-dimensional polymers. *Nature Chem* 2013;5:453-65. DOI
24. Zhao Y, Das S, Sekine T, et al. Record ultralarge-pores, low density threedimensional covalent organic framework for controlled drug delivery. *Angew Chem Int Ed* 2023;62:e202300172. DOI PubMed
25. Huang L, Yang J, Asakura Y, Shuai Q, Yamauchi Y. Nanoarchitectonics of hollow covalent organic frameworks: synthesis and applications. *ACS Nano* 2023;17:8918-34. DOI
26. Yang J, Huang L, You J, Yamauchi Y. Magnetic covalent organic framework composites for wastewater remediation. *Small* 2023;19:2301044. DOI PubMed
27. Liu K, Yang J, Liu J, et al. Robust self-floating covalent organic framework/chitosan aerogels for the efficient removal of sulfamerazine. *Chem Eng J* 2023;472:144966. DOI
28. Huang L, Yang J, Zhao Y, et al. Monolithic covalent organic frameworks with hierarchical architecture: attractive platform for contaminant remediation. *Chem Mater* 2023;35:2661-82. DOI
29. Zhang F, Ma X, Dong X, Miao X, Lang X. Inserting acetylene into an olefin-linked covalent organic framework for boosting the selective photocatalytic aerobic oxidation of sulfides. *Chem Eng J* 2023;451:138802. DOI
30. Huang N, Ding X, Kim J, Ihee H, Jiang D. A photoresponsive smart covalent organic framework. *Angew Chem Int Ed* 2015;54:8704-7. DOI PubMed PMC
31. Acharjya A, Pachfule P, Roeser J, Schmitt FJ, Thomas A. Vinylene-linked covalent organic frameworks by base-catalyzed aldol condensation. *Angew Chem Int Ed* 2019;58:14865-70. DOI PubMed PMC
32. Jadhav T, Fang Y, Liu CH, et al. Transformation between 2D and 3D covalent organic frameworks via reversible [2 + 2] cycloaddition. *J Am Chem Soc* 2020;142:8862-70. DOI PubMed
33. Zhu Y, Shao P, Hu L, et al. Construction of interlayer conjugated links in 2D covalent organic frameworks via topological polymerization. *J Am Chem Soc* 2021;143:7897-902. DOI PubMed
34. Ishii F, Matsunami S, Shibata M, Kakuchi T. *Cis-trans* isomerization and ^{13}C-NMR chemical shift of polyphenylacetylene. *J Polym Sci Part B Polym Phys* 1999;37:1657-64. DOI
35. Chan CYK, Tseng NW, Lam JWY, Liu J, Kwok RTK, Tang BZ. Construction of functional macromolecules with well-defined structures by indium-catalyzed three-component polycoupling of alkynes, aldehydes, and amines. *Macromolecules* 2013;46:3246-56. DOI
36. Terao T, Maeda S, Yamabe T, Akagi K, Shirakawa H. ^{13}C high-resolution NMR study of undoped polyacetylene. *Chem Phys Lett* 1984;103:347-51. DOI
37. Taniguchi T, Yoshida T, Echizen K, Takayama K, Nishimura T, Maeda K. Facile and versatile synthesis of end-functionalized poly(phenylacetylene)s: a multicomponent catalytic system for well-controlled living polymerization of phenylacetylenes. *Angew Chem Int Ed Engl* 2020;59:8670-80. DOI PubMed
38. Jin YJ, Kim H, Miyata M, et al. Influence of a hydrodynamic environment on chain rigidity, liquid crystallinity, absorptivity, and photoluminescence of hydrogen-bonding-assisted helical poly(phenylacetylene). *RSC Adv* 2016;6:36661-6. DOI
39. Shi G, Dai X, Xu Q, Shen J, Wan X. Enantioseparation by high-performance liquid chromatography on proline-derived helical polyacetylenes. *Polym Chem* 2021;12:242-53. DOI
40. Bontapalle S, Varughese S. Understanding the mechanism of ageing and a method to improve the ageing resistance of conducting PEDOT:PSS films. *Polym Degrad Stab* 2020;171:109025. DOI
41. Li JR, Zhou HC. Bridging-ligand-substitution strategy for the preparation of metal-organic polyhedra. *Nature Chem* 2010;2:893-8. DOI
42. Li J, Han X, Wang D, et al. A deprotection-free method for high-yield synthesis of graphdiyne powder with in situ formed cuo nanoparticles. *Angew Chem Int Ed* 2022;134:e202210242. DOI
43. Ma K, Wu J, Wang X, et al. Periodically interrupting bonding behavior to reformat delocalized electronic states of graphdiyne for improved electrocatalytic hydrogen evolution. *Angew Chem Int Ed Engl* 2022;134:e202211094. DOI PubMed
44. Zhuo S, Shi Y, Liu L, et al. Dual-template engineering of triple-layered nanoarray electrode of metal chalcogenides sandwiched with hydrogen-substituted graphdiyne. *Nat Commun* 2018;9:3132. DOI PubMed
45. Goldberg IB, Crowe HR, Newman PR, Heeger AJ, Macdiarmid AG. Electron spin resonance of polyacetylene and AsF_5-doped polyacetylene. *J Chem Phys* 1979;70:1132-6. DOI
46. Bernier P, Rolland M, Galtier M, et al. Electronic properties of non-doped and doped polyacetylene films studied by E.S.R. *J Phyique*

Lett 1979;40:297-301. DOI
47. Bartl A, Doege HG, Froehner J, Lehmann G, Pietrass B. Influence of iodine doping on ESR properties of polyacetylene. *Synth Met* 1984;10:151-6. DOI
48. Bartl A, Dunsch L, Park YW, Choi ES, Suh DS. Quantum transport in $AuCl_3$ doped polyacetylene studied by ESR. *Synth Met* 2001;117:21-5. DOI
49. Tang X, Chen Z, Xu Q, et al. Design of photothermal covalent organic frameworks by radical immobilization. *CCS Chem* 2022;4:2842-53. DOI
50. Komaba K, Goto H. Soliton excitations in liquid crystal polyacetylene. *Mol Cryst Liquid Crystals* 2020;703:69-78. DOI
51. Zhan X, Yang M, Shen Y, Wan M. Vibration and photoelectron spectroscopies of iodine-doped poly(*p*-diethynylbenzene). *Eur Polym J* 2002;38:2349-53. DOI
52. Weber J, Antonietti M, Thomas A. Microporous networks of high-performance polymers: elastic deformations and gas sorption properties. *Macromolecules* 2008;41:2880-5. DOI
53. Chen D, Chen W, Xing G, Zhang T, Chen L. An upgraded "two-in-one" strategy toward highly crystalline covalent organic frameworks. *Chem Eur J* 2020;26:8377-81. DOI PubMed
54. Egerton RF, Li P, Malac M. Radiation damage in the TEM and SEM. *Micron* 2004;35:399-409. DOI PubMed
55. Seo JM, Noh HJ, Jeong HY, Baek JB. Converting unstable imine-linked network into stable aromatic benzoxazole-linked one via post-oxidative cyclization. *J Am Chem Soc* 2019;141:11786-90. DOI PubMed
56. Smith BJ, Hwang N, Chavez AD, Novotney JL, Dichtel WR. Growth rates and water stability of 2D boronate ester covalent organic frameworks. *Chem Commun* 2015;51:7532-5. DOI PubMed
57. Pachfule P, Acharjya A, Roeser J, et al. Diacetylene functionalized covalent organic framework (COF) for photocatalytic hydrogen generation. *J Am Chem Soc* 2018;140:1423-7. DOI PubMed
58. Mondloch JE, Karagiaridi O, Farha OK, Hupp JT. Activation of metal-organic framework materials. *CrystEngComm* 2013;15:9258-64. DOI
59. Zhu D, Verduzco R. Ultralow surface tension solvents enable facile COF activation with reduced pore collapse. *ACS Appl Mater Interfaces* 2020;12:33121-7. DOI PubMed
60. Yokozawa T, Ohta Y. Transformation of step-growth polymerization into living chain-growth polymerization. *Chem Rev* 2016;116:1950-68. DOI PubMed
61. Miyatake K, Hlil AR, Hay AS. High molecular weight aromatic polyformals free of macrocyclic oligomers. A condensative chain polymerization reaction. *Macromolecules* 2001;34:4288-90. DOI
62. Chien JCW. Kinetics of acetylene polymerization and structures of polyacetylene. *Polym Eng Sci* 1985;25:635-42. DOI
63. Schen MA, Karasz FE, Chien JCW. Kinetics and mechanism of acetylene polymerization. *J Polym Sci Polym Chem Ed* 1983;21:2787-812. DOI
64. Basescu N, Liu ZX, Moses D, Heeger AJ, Naarmann H, Theophilou N. High electrical conductivity in doped polyacetylene. *Nature* 1987;327:403-5. DOI
65. Park YW, Heeger AJ, Druy MA, Macdiarmid AG. Electrical transport in doped polyacetylene. *J Chem Phys* 1980;73:946-57. DOI
66. Jin YJ, Kwak G. Properties, functions, chemical transformation, nano-, and hybrid materials of poly(diphenylacetylene)s toward sensor and actuator applications. *Polym Rev* 2017;57:175-99. DOI